The Propagation Characteristics of Signal Lines in a Mesh-Plane Environment

BARRY J. RUBIN, MEMBER, IEEE

Abstract—**This paper investigates the propagation characteristics of signal lines situated between a pair of mesh reference planes in a homogeneous dielectric. These mesh reference planes, which form the heart of high-performance multichip modules, provide a transmission-line environment for the signals carried between integrated circuit chips.**

A numerical solution that employs a set of rooftop functions to represent the current density is developed and used to find the propagation velocity and characteristic impedance in mesh-plane structures where the conductors have zero thickness and finite sheet resistance. The telegraphist's equations are shown to apply, and are used to find the capacitance and inductance matrices in coupled line configurations. The near- and far-end crosstalk are calculated when the coupled lines are on the same, and on opposite, sides of a mesh plane. The presence of conductors which run in a direction orthogonal to the signal lines, whether as an array of crossing signal lines or as part of the mesh planes, is shown to significantly affect only the capacitive parameters. The influence of such orthogonal lines on the propagation velocity, characteristic impedance, and crosstalk are given, and a detailed plot clearly indicates the circulating current flow in these lines.

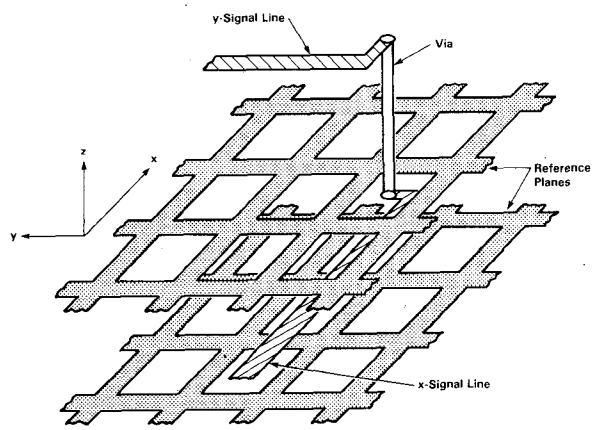

Fig. 1. Section of multi-chip module showing reference planes, and signal lines interconnected through a via.

I. Introduction

TRANSMISSION LINES in the form of signal lines embedded in a dielectric and sandwiched between conductive reference planes are used in high-performance computers to carry signals between integrated circuit chips. A compact multichip carrier, or module, may be constructed by stacking such conductor-dielectric sandwiches, where the reference planes and dielectric are perforated so that signal lines can be connected to the chips at the module's top surface, to pins on the module's surface, or to signal lines located on other layers. A module that can hold 100 chips has been described in [1].

A section of such a module is shown in Fig. 1. Here, a signal line situated between a pair of perforated (mesh) reference planes is connected to another signal line through a conductive element called a via. Generally, each signal layer, which consists of lines running in only one direction, is accompanied by a second layer having lines oriented in the orthogonal direction. At least one pair of signal layers is placed between mesh planes, though crosstalk and impedance constraints may limit this number to two.

A search of the literature reveals no comprehensive analysis of the above structure, though propagation along a pair of wire meshes [2] and the effect of orthogonal, or crossing, lines on signal lines situated between perfect ground planes [3] have been investigated. In this paper, we extend the analysis presented in [4], where guided wave solutions are found for signal lines situated above one periodically perforated ground plane to include a second such plane and an array of orthogonal signal lines. The propagation velocity, characteristic impedance, and signal-line crosstalk are calculated, and numerical results presented. The effect of crossing signal lines is discussed in detail.

Manuscript received August 30, 1983; revised January 16, 1984.

The author is with the General Technology Division of the IBM Corporation, Hopewell Junction, NY 12533.

II. Solution Technique

The structure considered is shown in Fig. 2, where a pair of signal layers is situated between two mesh planes. The conductors have zero thickness and finite sheet resistance $R_s \geq 0$, and the supporting medium, which extends throughout all space, has relative dielectric constant ϵ_r. The mesh planes, formed from intersecting conductive strips of widths w_x and w_y, have periodicities d_1 and d_{2m} in the x and y directions, respectively, and are located at $z = 0$ and $z = h_3$. The x- and y-signal lines have widths w_y and w_x, respectively, and are situated at $z = h_1$ and $z = h_2$. Consistent with typical computer packages, the signal lines and mesh planes are so aligned that their projections on the plane $z = 0$ coincide. The x- and y-lines initially are assumed to be arrays with respective periodicities of d_2 and d_1 (so the periodicities defining the entire structure are d_2 and d_1), but through antisymmetric excitation of the x-signal lines, the periodicity in the y direction will be removed. In the following, k_ϵ and η_ϵ are the wave number and the wave impedance in the dielectric, the time dependency is $\exp(j\omega t)$ where ω is the angular frequency, and x is the

0018-9480/84/0500-0522$01.00 ©1984 IEEE

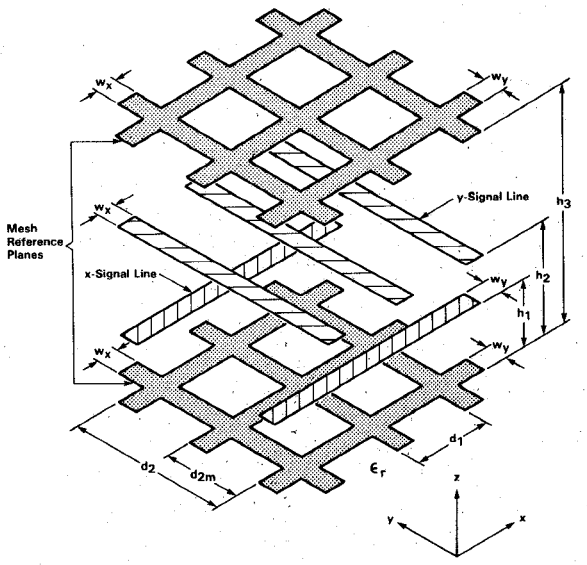

Fig. 2. Transmission line structure having arrays of x- and y-signal lines situated between a pair of mesh reference planes.

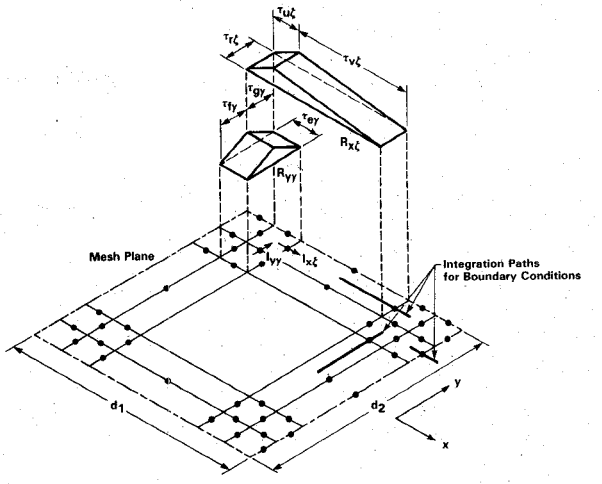

Fig. 3. Unit cell of mesh plane, indicating rooftop functions used to approximate current density and line intervals over which boundary conditions are applied.

direction of propagation. The terms y-signal lines and crossing lines will be used interchangeably.

A. Eigensolution for an Array of Signal Lines Above a Mesh Plane

Reference [4] presents a solution for a structure having only x-signal lines and one mesh plane. The current density $\underline{J}_s$, within a suitably defined unit cell that includes both signal line and mesh plane, is approximated as a linear combination of rooftop functions [4]–[6] multiplied by the factor $\exp(-jk_x x)$, where k_x is the propagation constant. The transverse component of electric field $\underline{E}_t$ is expressed in terms of the current using [6], and the electric field boundary condition

$$\underline{E}_t - \underline{J}_s R_s = 0 \tag{1}$$

is then integrated along appropriate line segments on the conductor, generating the set of equations

$$\sum_{\alpha=1}^{P} I_{x\alpha}\left(Z_{xx\alpha\beta} - R_s F_{x\alpha\beta}\right) + \sum_{\alpha=1}^{Q} I_{y\alpha} Z_{xy\alpha\beta} = 0, \qquad \beta = 1,2,\cdots,P$$

$$\sum_{\alpha=1}^{P} I_{x\alpha} Z_{yx\alpha\beta} + \sum_{\alpha=1}^{Q} I_{y\alpha}\left(Z_{yy\alpha\beta} - R_s F_{y\alpha\beta}\right) = 0, \qquad \beta = 1,2,\cdots,Q \tag{2}$$

where $I_{x\alpha}$, $I_{y\alpha}$ are complex current coefficients, the Z elements are infinite series, and P and Q are, respectively, the number of rooftop current elements required to approximate J_{sx} and J_{sy}. The determinantal equation associated with (2) is solved, yielding k_x; k_x is then substituted back into (2) to give $I_{x\alpha}$, $I_{y\alpha}$ and thus the current density.

B. Extension of Single Mesh-Plane Analysis

We find the solution associated with the structure of Fig. 2 by including in the analysis the current density on the conductors located at $z = h_2$ and $z = h_3$. In addition, we employ rooftop functions that are not necessarily symmetrical along the direction of current flow. The use of such asymmetrical rooftop functions relaxes the dependencies between the geometrical parameters w_x, w_y, d_1, and d_2 that would otherwise result, and allows the current density to be represented with fewer current elements.

The rooftop functions are shown in Fig. 3, where their use in representing the mesh current density of a structure where $d_{2m} = d_2$ is indicated. As in [4], the dots define the centers of the rooftop functions, being omitted at redundant points along the unit cell boundary, and the heavy lines define some line segments over which (1) is integrated to obtain (2). The use of asymmetrical rooftop functions, however, results in a subdivision of the unit cell which is not a uniform rectangular grid. The dimensions of the rectangles are fixed by the parameters $\tau_{u\alpha}$, $\tau_{v\alpha}$, and $\tau_{r\alpha}$, which define $R_{x\alpha}(x - x_\alpha, y - y_\alpha)$, the x-directed rooftop function centered at $(x_\alpha, y_\alpha, z_\alpha)$, and by the parameters $\tau_{e\alpha}$, $\tau_{f\alpha}$, and $\tau_{g\alpha}$, which define $R_{y\alpha}(x - x_{P+\alpha}, y - y_{P+\alpha})$, the y-directed rooftop function centered at $(x_{P+\alpha}, y_{P+\alpha}, z_{P+\alpha})$.

The resulting Z coefficients of (2) associated with the structure of Fig. 2 are then

$$Z_{xx\alpha\beta} = -\frac{\eta_\epsilon}{2k_\epsilon} \sum_{n,m} S\left(k_{xn}, \tau_{u\beta}, \tau_{v\beta}\right) \cdot \frac{k_\epsilon^2 - k_{xn}^2}{k_{znm}} \mathcal{R}_{xnm\alpha} \exp\left\{ j\left[\frac{2\pi n}{d_1}(x_\alpha - x_\beta) + \frac{2\pi m}{d_2}(y_\alpha - y_\beta) - k_{znm}|z_\alpha - z_\beta| \right] \right\}$$

$$Z_{xy\alpha\beta} = \frac{\eta_\epsilon}{2k_\epsilon} \sum_{n,m} S\left(k_{xn}, \tau_{u\beta}, \tau_{v\beta}\right) \cdot \frac{k_{xn} k_{ym}}{k_{znm}} \mathcal{R}_{ynm\alpha} \exp\left\{ j\left[\frac{2\pi n}{d_1}(x_{P+\alpha} - x_\beta) + \frac{2\pi m}{d_2}(y_{P+\alpha} - y_\beta) - k_{znm}|z_{P+\alpha} - z_\beta| \right] \right\}$$

$$Z_{yx\alpha\beta} = \frac{\eta_\epsilon}{2k_\epsilon} \sum_{n,m} S(k_{ym}, \tau_{f\beta}, \tau_{g\beta}) \cdot \frac{k_{xn}k_{ym}}{k_{znm}} \mathscr{R}_{xnm\alpha} \exp\left\{ j\left[\frac{2\pi n}{d_1}(x_\alpha - x_{P+\beta}) + \frac{2\pi m}{d_2}(y_\alpha - y_{P+\beta}) - k_{znm}|z_\alpha - z_{P+\beta}| \right] \right\}$$

$$Z_{yy\alpha\beta} = -\frac{\eta_\epsilon}{2k_\epsilon} \sum_{n,m} S(k_{ym}, \tau_{f\beta}, \tau_{g\beta}) \cdot \frac{k_\epsilon^2 - k_{ym}^2}{k_{znm}} \mathscr{R}_{ynm\alpha} \exp\left\{ j\left[\frac{2\pi n}{d_1}(x_{P+\alpha} - x_{P+\beta}) + \frac{2\pi m}{d_2}(y_{P+\alpha} - y_{P+\beta}) - k_{znm}|z_{P+\alpha} - z_{P+\beta}| \right] \right\} \tag{3}$$

where

$$k_{xn} = k_x + \frac{2\pi n}{d_1} \qquad k_{ym} = \frac{2\pi m}{d_2}$$

$$k_{znm} = \left(k_\epsilon^2 - k_{xn}^2 - k_{ym}^2\right)^{1/2}$$

$$S(k, \tau_u, \tau_v) = \frac{\exp(-jk\tau_v/2) - \exp(jk\tau_u/2)}{-jk}$$

and $\mathscr{R}_{xnm\alpha}$ and $\mathscr{R}_{ynm\alpha}$ are the Fourier series coefficients of $R_{x\alpha}(x, y)$ and $R_{y\alpha}(x, y)$, respectively. Though resistive structures can be handled, in this paper we present examples only for conductors having $R_s = 0$; the F elements of (2), therefore, are not needed, but for reference are included in the Appendix.

C. Application of Symmetry

The reference planes in high-performance modules are generally interconnected directly through vias, or indirectly through paths which may include vias, power supply pins, decoupling capacitors, and logic circuits. These elements serve to short the mesh planes together, precluding the possibility of a time-varying potential difference between the mesh planes and thus preventing the existence of a mode corresponding to this potential difference. On the other hand, such elements greatly complicate the analysis.

To short the mesh planes but not overly complicate the problem, we force the x-directed current I in adjacent x-signal lines to flow in opposite directions so by symmetry the tangential electric field is zero along the $x-z$ planes midway between these lines. The unit cell, as shown in Fig. 4(a), includes two x-signal lines and has periodicity $2d_2$ in the y direction. (This requires that d_2 be replaced by $2d_2$ in (3) and its auxiliary equations.) Since the tangential electric field is zero along the planes indicated in the figure, perfectly conducting walls may be placed there without disturbing the field. A reduced unit cell having periodicity d_2 in the y direction may then be defined, as shown in Fig. 4(b). In fact, the structure no longer needs to be considered as periodic in the y direction since the conducting walls totally isolate the structure in this direction. Also observe

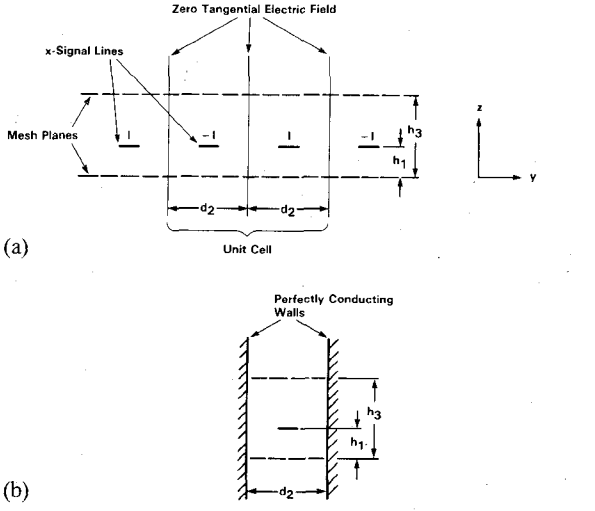

Fig. 4. Transmission line structure where adjacent x-signal lines carry current in opposite directions. (a) Section of structure showing unit cell and planes where the tangential electric field is zero. (b) Reduced unit cell.

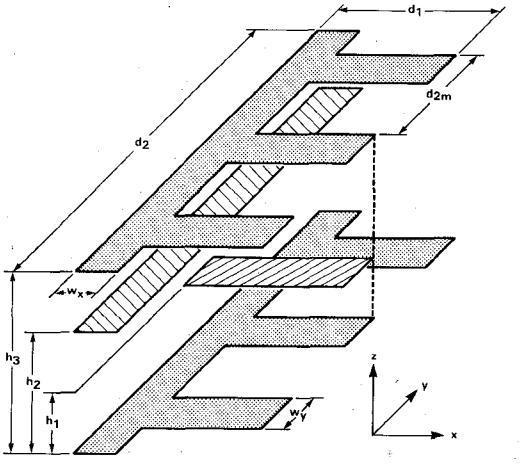

Fig. 5. Isometric view of the reduced unit cell (Fig. 4(b)) when $d_2 = 3d_{2m}$.

that only one propagation constant is associated with this structure. Had the mesh planes not been shorted, the unit cell would have consisted of three nontouching conductors (an x-signal line and two mesh planes) so that the structure would have been a coupled transmission line possessing two distinct propagation constants.

Although the electric walls are necessary to short the reference planes, they do not actually exist in the module. To prevent these walls from significantly affecting the propagation characteristics, the distance between each x-signal line and the nearest wall must be large in comparison to the distance between the x-signal line and the nearest mesh plane. For typical structures, this may be accomplished by requiring the reduced unit cell width d_2 to be several times the periodicity of the mesh in the y direction, d_{2m}.

Fig. 5 gives an isometric view of the unit cell (subsequently, the term unit cell will be taken to mean reduced unit cell) when $d_2 = 3d_{2m}$. The y-signal line shown included in the figure may or may not actually be present. A

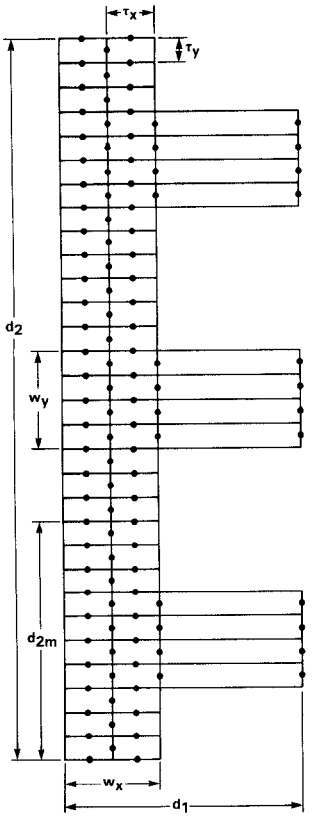

Fig. 6. Subdivision of mesh plane suitable for unit cell of Fig. 5.

particular subdivision of this unit cell suitable for the examples to be presented is shown in Fig. 6. The unit cell is divided along y into uniform segments of length τ_y; along x the unit cell is divided into two equal segments of length τ_x and a third segment of length $d_1 - w_x$. Though shown explicitly only for the mesh planes, subdivisions may be obtained for the x- and y-signal lines from their projection onto the grid shown. The dots indicate the centers of the rooftop functions employed in the representation of the current density.

III. Characteristic Impedance

A characteristic impedance Z_0 can be defined for this structure. Since the current and voltage are the variables generally encountered in the analysis of computer circuits, it is convenient to define Z_0 as

$$Z_0 = V/I \tag{4}$$

where V is the voltage difference between the x-signal line and a mesh plane (generally the mesh plane at $z = 0$), and I is the total x-directed current in the x-signal line. As described in [4], V can be obtained by integrating the z component of the electric field between the signal line and a mesh plane, though this voltage depends on the integration path because the wave is non-TEM. In typical mesh-plane structures, however, the wave is nearly TEM and the ambiguity in voltage so small that the utility of V is not impaired. Modifying the analysis of [4] to include the

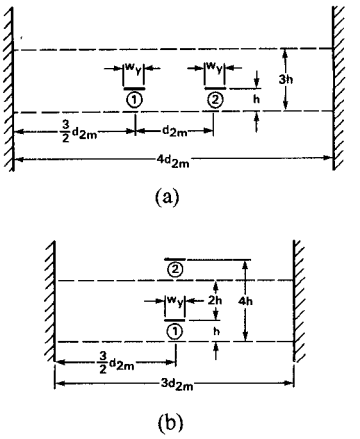

Fig. 7. Configurations used in coupling analysis. (a) Unit cell for side-by-side coupling. (b) Unit cell for through-mesh coupling.

y-signal line and the second mesh plane, we find

$$Z_0 = j\frac{\eta_\epsilon}{2k_\epsilon}\left[\sum_{\alpha=1}^{P} I_{x\alpha}\sum_{n,m} G_{xnm\alpha}\cdot\frac{\exp(-jk_{znm}|z_\alpha|)-\exp(-jk_{znm}|z_\alpha - h_1|)}{k_{znm}} + \sum_{\alpha=1}^{Q} I_{y\alpha}\sum_{n,m} G_{ynm\alpha}\cdot\frac{\exp(-jk_{znm}|z_{P+\alpha}|)-\exp(-jk_{znm}|z_{P+\alpha}-h_1|)}{k_{znm}}\right]\cdot\left[\sum_{\alpha=1}^{P} I_{x\alpha}\tau_{r\alpha}\delta_{h_1,z_\alpha}q_{\tau_{u\alpha},\tau_{v\alpha}}(x-x_\alpha)\right]^{-1} \tag{5}$$

where

$$G_{xnm\alpha} = k_{xn}\mathscr{R}_{xnm\alpha}\exp\left\{j\left[\frac{2\pi n}{d_1}(x_\alpha - x)+\frac{2\pi m}{d_2}(y_\alpha - y)\right]\right\}$$

$$G_{ynm\alpha} = k_{ym}\mathscr{R}_{ynm\alpha}\cdot\exp\left\{j\left[\frac{2\pi n}{d_1}(x_{P+\alpha} - x)+\frac{2\pi m}{d_2}(y_{P+\alpha} - y)\right]\right\}.$$

$\delta_{u,v}$ is a modified form of the Kronecker delta, defined in the Appendix, and $q_{u,v}$ is a function having the triangle dependency of the x-directed rooftop function (Fig. 3). When adjacent x-signal lines are oppositely excited, (4) and (5) are modified to reflect the new unit cell.

IV. Signal-Line Coupling and Crosstalk

The crosstalk between two adjacent signal lines can be obtained by modifying the unit cell of Fig. 4(b) so that it contains two x-signal lines, finding the associated capacitance and inductance matrices, and then substituting the appropriate matrix elements into well-known formulas for the near- and far-end coupled noise. Since the reference planes are meshes, not solid planes, coupling will exist between lines located on the same, and on opposite, sides of a mesh plane. Subsequently, two unit cells need to be defined.

Fig. 7(a) shows a unit cell suitable for finding the crosstalk between horizontally adjacent signal lines (side-by-side case). A second unit cell, suitable for finding the crosstalk between signal lines separated by a mesh plane (through-mesh case) is shown in Fig. 7(b). In each cell, the x-signal lines (labeled 1 and 2) are a distance $3d_{2m}/2$ from the nearest electric wall. Crossing lines will be considered only in the side-by-side structure.

The total x-directed currents in the two coupled x-signal lines I_1 and I_2, and the potential differences between these lines and the nearest mesh planes V_1 and V_2 (found through integration of the z-directed electric field), are calculated for each propagating mode associated with the structure. As opposed to a TEM structure, where only one propagation constant (and hence only one mode) may exist, a mesh structure having two signal lines supports two distinct propagation constants (and hence two modes). The proportion of each mode present depends upon the boundary conditions (voltages and terminations) imposed at the ends of the signal lines. The parameters I_1, I_2, V_1, and V_2 are then substituted into the telegraphist's equations [7] (which we assume and later verify to hold for our structure), which in matrix form and expressed through phasors are

$$-jk_x^i \boldsymbol{V}^i = -j\omega L \boldsymbol{I}^i \tag{6a}$$

$$-jk_x^i \boldsymbol{I}^i = -j\omega C \boldsymbol{V}^i \tag{6b}$$

where

$$\boldsymbol{V} = \begin{bmatrix} V_1 \\ V_2 \end{bmatrix} \qquad \boldsymbol{I} = \begin{bmatrix} I_1 \\ I_2 \end{bmatrix}$$

and C and L are the per unit length capacitance and inductance matrices

$$C = \begin{bmatrix} C_{11} & -C_{12} \\ -C_{21} & C_{22} \end{bmatrix} \tag{7a}$$

$$L = \begin{bmatrix} L_{11} & L_{12} \\ L_{21} & L_{22} \end{bmatrix}. \tag{7b}$$

The superscript i, which may be either 1 or 2, denotes the mode. Since two modes exist, (6a) represents a set of four equations in the four unknowns L_{11}, L_{12}, L_{21}, and L_{22}; (6b) represents a set of four equations in the four unknowns C_{11}, C_{12}, C_{21}, and C_{22}. Hence, both C and L can be obtained from (6).

From [8] and [9], the saturated near-end noise V_N and far-end noise V_F, in ideal transmission lines with pulse excitation, may be expressed as

$$V_N = \frac{1}{4}(K_C + K_L)V_S \tag{8a}$$

$$V_F = \frac{1}{2} l\sqrt{L_{11}C_{11}}\,(K_C - K_L)V_S/\tau \tag{8b}$$

where V_S is the voltage amplitude on the active line, l is the coupled length, τ is the input pulse risetime, and K_C and K_L are the capacitive and inductive coupling coefficients, which may be expressed as

$$K_C = C_{12}/\sqrt{C_{11}C_{22}} \tag{9a}$$

$$K_L = L_{12}/\sqrt{L_{11}L_{22}}\,. \tag{9b}$$

Equations (8a) and (8b) apply to coupled lines which are terminated in impedances $\sqrt{L_{ii}/C_{ii}}$, $i=1, 2$. Viewing the voltage waveform in the structure as a superposition of two waves having distinct propagation velocities and which repeatedly reflect (to a small degree) off the ends of the lines [7], these equations are seen to be approximations—in [9], such equations are stated as valid when the lines are loosely coupled and l is nonexcessive. Actually, (8b) is valid only when the difference in propagation delay along l of the two modes is less than τ. A further restraint on (8), when applied to the periodic structure considered here, is that the input pulse not distort as it propagates—this requires $1/\tau$ to be small compared to the structure's cutoff frequency. For typical computer modules, all the above-mentioned constraints are satisfied, and (8) gives reasonably accurate results.

V. Numerical Results

A. Calculation of Propagation Characteristics for Two-Mesh-Plane Structures

A number of examples are now considered. In each, the parameters w_x and w_y are chosen to allow a unit cell subdivision as shown in Fig. 6, though the number of intervals of length τ_y along the y direction may differ from that shown. The infinite series in (3) and (5) are truncated after $|n| = N$ and $|m| = M$, where N and M are the smallest integers satisfying

$$N \geq \max\left(\frac{d_1}{\tau_x}, \frac{d_1}{d_1 - w_x}\right)$$

$$M \geq \frac{2d_2}{\tau_y} \tag{10}$$

and both τ_x and τ_y are intervals as depicted in Fig. 6. This choice for N and M guarantees that at least one period of the highest Fourier series mode of any rooftop function will fit into each rectangle shown in Fig. 6.

As in [4], the propagation constant k_x, which appears implicitly in the determinantal equation (2), is obtained through a Newton search. We define the normalized propagation velocity $\hat{v}$ as the propagation velocity divided by the speed of light in the dielectric. At low frequency ($k_\epsilon d_1 \ll 1$) in perfectly conducting structures, $\hat{v}$ may be simply expressed as

$$\hat{v} = k_\epsilon / k_x.$$

In the following examples, $R_s = 0, \epsilon_r = 10$ (consistent with alumina ceramic dielectrics), $k_\epsilon = 0.006$ mm^{-1}, and the structures are such that $h_1 = h$, $h_2 = 2h$, and $h_3 = 3h$. Since $R_s = 0$ and $k_\epsilon d_1$ will be sufficiently small, k_x, $\hat{v}$, and Z_0 will be real. The characteristic impedance and voltages in all the examples are calculated at the point along the line bisecting the x-signal line, midway between the y-directed conducting strips that constitute the mesh planes. Such a choice has been found to yield the most accurate values of the capacitance and inductance matrices. The first example deals with the effect of the electric walls on the propagation characteristics.

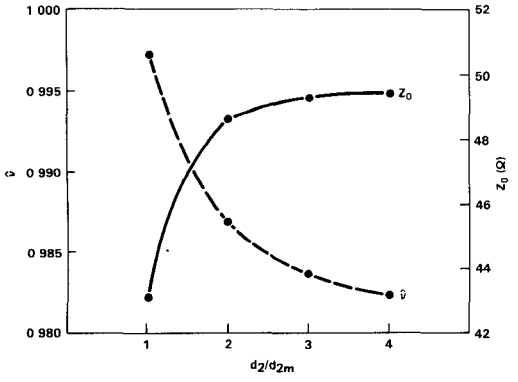

Fig. 8. Normalized propagation velocity ($\hat{v}$) and characteristic impedance (Z_0) against d_2/d_{2m} for the structure of Fig. 2 having no crossing lines ($k_\epsilon = 0.006$ mm^{-1}, $\epsilon_r = 10$, $R_s = 0$, $d_1 = d_{2m} = 0.5$ mm, $h = 0.2$ mm, $w_x = w_y = 0.125$ mm, $\tau_x = 0.0625$ mm, $\tau_y = 0.03125$ mm).

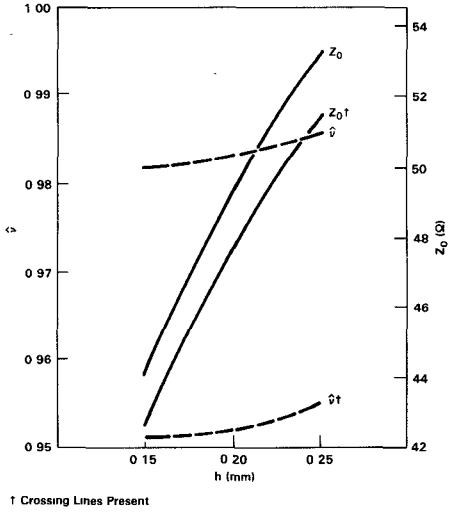

Fig. 9. Normalized propagation velocity ($\hat{v}$) and characteristic impedance (Z_0) against h for the structure of Fig. 5 ($k_\epsilon = 0.006$ mm^{-1}, $\epsilon_r = 10$, $R_s = 0$, $d_1 = d_{2m} = 0.5$ mm, $d_2 = 1.5$ mm, $w_x = w_y = 0.125$ mm, $\tau_x = 0.0625$ mm, $\tau_y = 0.03125$ mm).

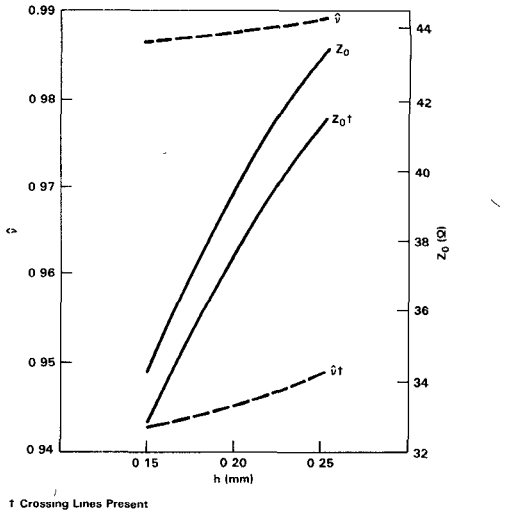

Fig. 10. Normalized propagation velocity ($\hat{v}$) and characteristic impedance (Z_0) against h for the structure of Fig. 5 ($k_\epsilon = 0.006$ mm^{-1}, $\epsilon_r = 10$, $R_s = 0$, $d_1 = d_{2m} = 0.5$ mm, $d_2 = 1.5$ mm, $w_x = w_y = 0.2$ mm, $\tau_x = 0.1$ mm, $\tau_y = 0.05$ mm).

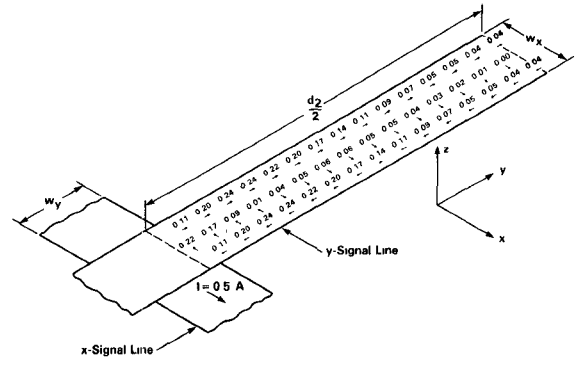

Fig. 11. Current density (A/mm) in y-signal line of half the unit cell of Fig. 5 when $I = 0.5$ A ($k_\epsilon = 0.006$ mm^{-1}, $\epsilon_r = 10$, $R_s = 0$, $d_1 = d_{2m} = 0.5$ mm, $d_2 = 1.5$ mm, $h = 0.15$ mm, $w_x = w_y = 0.2$ mm, $\tau_x = 0.1$ mm, $\tau_y = 0.05$ mm).

As discussed earlier, d_2/d_{2m} must be large enough to prevent the electric walls in the unit cell (Fig. 4(b)) from significantly affecting the propagation characteristics. The variation of $\hat{v}$ and Z_0 with d_2/d_{2m} is presented in Fig. 8 for the structure of Fig. 2 (with no crossing lines) when $w_x = w_y = 0.125$ mm, $d_1 = d_{2m} = 0.5$ mm, $h = 0.2$ mm, $\tau_x = 0.0625$ mm, and $\tau_y = 0.03125$ mm (remember that $R_s = 0$, $\epsilon_r = 10$, and $h_1 = h$, $h_2 = 2h$, $h_3 = 3h$). The unit cell (Fig. 5) and its subdivision (Fig. 6), though valid for $d_2/d_{2m} = 3$, are appropriately modified for other values of d_2/d_{2m}. We observe that $\hat{v}$ monotonically decreases and Z_0 monotonically increases with d_2/d_{2m}, but both saturate around $d_2/d_{2m} = 3$. Thus, for structures having h about 0.2 mm, we can expect $d_2/d_{2m} = 3$ to be sufficient for reasonable accuracy.

The impedance and normalized propagation velocity are plotted against h in Fig. 9 for the structure of Fig. 5 when d_2/d_{2m} is fixed at 3, but with the other geometrical parameters as given above. We observe that $\hat{v}$ and Z_0 increase with h over the given range, and both decrease by about 3 percent when crossing lines (y-signal lines) are introduced. These y-signal lines, spaced at intervals of d_1, form a periodic array of capacitive discontinuities and thus increase the capacitance of the x-signal line, lowering the impedance and slowing the wave. Although $\hat{v}$ increases with h, apparently due to the increasing effect of the conducting walls, when h approaches zero one would expect the wave to approach TEM and $\hat{v}$ to increase to unity. Thus, the sensitivity of $\hat{v}$ to h over the range $h = 0$ to $h = 0.15$ mm may not be intuitively clear.

Fig. 10 gives $\hat{v}$ and Z_0 against h for the same structure, except $w_x = w_y = 0.2$ mm, and the subdivision parameters are $\tau_x = 0.1$ mm and $\tau_y = 0.05$ mm. Consistent with wider lines, Z_0 is smaller, $\hat{v}$ is greater (the wave is more nearly TEM), and the effect of crossing lines on both parameters is greater. The current density in the y-signal line when $h = 0.15$ mm and the x-signal line carries a current of 0.5 A is shown for half the unit cell in Fig. 11. As expected, the current flows in loops to cancel the magnetic field within the line that is produced by the mesh planes and x-signal line. For the half unit cell shown, the current flows in the clockwise direction, but by symmetry flows counterclockwise in the other half. The current flow in a mesh plane, though for a simpler structure, is given in [4].

TABLE I
COMPARISON OF CAPACITIVE AND INDUCTIVE PARAMETERS IN COUPLING STRUCTURES
$k_\epsilon = 0.006$ mm^{-1}, $\epsilon_r = 10$, $R_s = 0$, $d_1 = d_{2m} = 0.5$ mm, $h = 0.2$ mm, $w_x = w_y = 0.125$ mm, $\tau_x = 0.0625$ mm, $\tau_y = 0.03125$ mm

Coupling Configuration	C_{11} (pf/mm)	C_{12} (pf/mm)	C_{21} (pf/mm)	C_{22} (pf/mm)	L_{11} (nh/mm)	L_{12} (nh/mm)	L_{21} (nh/mm)	L_{22} (nh/mm)
Side-by-Side*	0 2194	0 01837	0 01837	0 2194	0 5101	0 04271	0 04271	0 5101
Side-by-Side	0 2161	0 01338	0 01338	0 2161	0 5344	0 04189	0 04189	0 5344
Side-by-Side†	0 2307	0 00899	0 00899	0 2307	0 5337	0 04212	0 04212	0 5337
Through-Mesh*	0 2183	0 00700	0 00700	0 2076	0 5095	0 01718	0 01718	0 5357
Through-Mesh	0 2172	0 00333	0 00328	0 2062	0 5289	0 01721	0 01697	0 5554

* TEM Structure
† Crossing Lines Present

In Section IV, the telegraphist's equations were assumed to apply to the structures of Fig. 7(a) and (b) and were used to obtain the C and L matrices. We now show that this approach is valid by finding the C and L matrices associated with structures having no y-directed conductors, and then comparing these matrices to those obtained through (6) for the structures having y-directed conductors. The structures of Fig. 7(a) and (b), having no y-signal lines or y-directed conductors in the reference planes (so the meshes become arrays of x-directed conductors), support purely TEM waves, so that the associated capacitance matrices may be obtained using [10]. The inductance matrices, since the structures are TEM, can be obtained by inverting the C matrices and dividing the resulting matrix elements by the square of the velocity of light in the dielectric.

Table I gives the elements of the L and C matrices calculated for the structures of Fig. 7(a) and (b) as shown and for their TEM counterparts, when $h = 0.2$ mm, $w_x = w_y = 0.125$ mm, and $d_1 = d_{2m} = 0.5$ mm. We expect the presence of y-directed conductors to substantially reduce the mutual capacitances C_{12} and C_{21}, but to affect only slightly the other parameters. We now compare each parameter calculated for the TEM structure with the same parameter calculated for the mesh structure.

For the side-by-side case, we observe that the mutual inductances L_{12} and L_{21} agree to within 2.0 percent; the self inductances L_{11} and L_{22} agree to within 4.8 percent; C_{12} and C_{21} are substantially less, and the self capacitances C_{11} and C_{22} slightly less for the mesh structure. Though the changes in the self terms are in directions opposite to that expected (when y-conductors are added to a TEM structure, C_{11} and C_{22} should increase, while L_{11} and L_{22} should decrease), these slight discrepancies fall within the numerical uncertainty associated with the expansion and testing procedures employed—at the low frequencies considered here, the rooftop current expansion results in an essentially stepwise-constant charge distribution, and the line integral testing (of the electric field) actually results in a point testing of the voltage on the conductors. As shown in [11], when constant charge patches and point testing are used in finding the capacitance of a rectangular parallel-plate capacitor, the values calculated (against the number of subsections) approach the exact value from below. It is expected, then, considering the relatively coarse subdivision of the mesh structure ($\tau_x = 0.0625$ mm, $\tau_y = 0.03125$ mm) that the self capacitances be less and the self inductances (which vary inversely with the self capacitances) be greater. This behavior is further demonstrated in the section on numerical convergence. The mutual terms, which depend on the current (or charge) at one conductor and the field at another, are less affected by the particular subdivision.

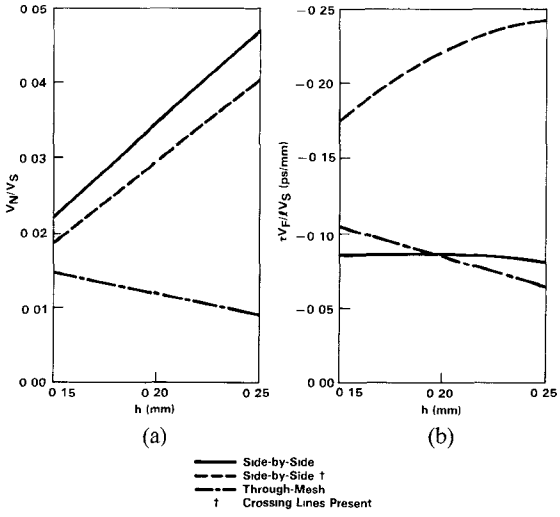

Fig. 12. Signal-line crosstalk against h. (a) Normalized saturated near-end noise. (b) Normalized far-end noise.

In the third row of Table I, crossing lines are considered in the side-by-side structure. These lines, acting as capacitive discontinuities, increase C_{11} and C_{22}, decrease C_{12} and C_{21}, but insignificantly change the inductances. The entries for the through-mesh case show excellent agreement (between the TEM and mesh structures) of the mutual inductances; the mutual capacitances are substantially less in the mesh structure, and the self terms are only slightly affected, though the changes again are in a direction other than expected. We observe that $C_{12} \neq C_{21}$ and $L_{12} \neq L_{21}$ in the mesh structure, in apparent violation of reciprocity. But the structure is not TEM so that the voltages used in (6) are somewhat ambiguous, being dependent on the integration path; therefore, reciprocity does not apply to these parameters. The exceptionally close agreement between L_{12} and L_{21}, and between C_{12} and C_{21}, however, further supports the application of the telegraphist's equations. For the side-by-side case, the symmetry of the structure forces $L_{12} = L_{21}$, and $C_{12} = C_{21}$, $C_{11} = C_{22}$, and $L_{11} = L_{22}$. Though Table I presents results for structures having $h = 0.2$ mm, calculations for $h = 0.15$ mm and $h = 0.25$ mm show the same excellent agreement and observed trends between the calculated parameters for the TEM and mesh structures.

The parameters of Table I, calculated for $h = 0.15$, 0.20, and 0.25 mm, are substituted into (8) and (9) to obtain the normalized saturated near-end noise (V_N/V_S) and the normalized far-end noise [$\tau V_F/(lV_S)$], for the side-by-side and through-mesh structures. Line 2 is the active line and the noise on line 1 will be determined (see Fig. 7). As shown in Fig. 12(a), the saturated near-end noise is greater for the

TABLE II
CONVERGENCE OF PROPAGATION VELOCITY, CHARACTERISTIC IMPEDANCE, CAPACITANCE, AND INDUCTANCE AGAINST THE NUMBER OF SUBDIVISIONS FOR A ONE-MESH-PLANE STRUCTURE (NO Y-SIGNAL LINES)
$k_\epsilon = 0.006$ mm^{-1}, $\epsilon_r = 10$, $R_s = 0$, $d_1 = d_{2m} = 0.5$ mm, $d_2 = 1.5$ mm, $h = 0.2$ mm, $w_x = w_y = 0.2$ mm.

Case	S_{x1}	S_{x2}	S_y	$\hat{v}$	Z_0 (Ω)	C (pf/mm)	L (nh/mm)
1	2	1	30	0 98829	42 04	0 2537	0 4484
2	2	1	60	0 98891	41 11	0 2593	0 4382
3	2	1	90	0 98913	40 79	0 2613	0 4347
4	2	1	120	0 98918	40 56	0 2627	0 4322
5	4	3	30	0 98907	41 97	0 2539	0 4473
6	4	3	60	0 98971	41 04	0 2595	0 4371

side-by-side case, even when crossing lines are introduced. The far-end noise (which is negative since $K_L > K_C$), as shown in Fig. 12(b), in both structures agree to within 20 percent. Once y-signal lines are introduced into the side-by-side structure, however, the reduction in C_{12} (and the corresponding decrease in coupling coefficient K_C) causes the far-end noise to substantially increase, well beyond that of either structure having no crossing lines. Though the variation with h of the near-end noise is intuitively obvious, the variation of the far-end noise, which depends on the difference between K_C and K_L, is more difficult to predict. This is made evident by the curves in Fig. 12(b). Though not shown, the corresponding TEM structures have noticeably larger near-end noises (since they have larger values of K_C), but no far-end noise (since $K_C = K_L$).

B. Numerical Convergence

We now investigate the convergence of the solution technique by choosing a convenient structure, varying the numbers of subsections and modes, and observing the changes in $\hat{v}$ and Z_0. The structure chosen must be simple enough to allow at least a four times increase in the number of subsections without leading to excessive computational cost—a suitable structure is a modified version of that considered in Fig. 10, having only one mesh plane (at $z = 0$) and no y-signal lines. The corresponding unit cell subdivision (Fig. 6) is modified so that S_{x1} equal intervals subdivide the x region of length w_x, S_{x2} equal intervals subdivide the x region of length $d_1 - w_x$, and S_y equal intervals subdivide the y region of length d_2. The original subdivision, then, corresponds to $S_{x1} = 2$, $S_{x2} = 1$, and $S_y = 30$. This new subdivision scheme requires (10), the expressions defining N and M, to be modified as follows:

$$N \geq \max\left(\frac{S_{x1}d_1}{w_x}, \frac{S_{x2}d_1}{d_1 - w_x}\right)$$
$$M \geq 2S_y. \tag{11}$$

Table II gives $\hat{v}$ and Z_0 for a number of different subdivisions. We observe, from cases 1 through 4, that both $\hat{v}$ and Z_0 vary monotonically and converge as S_y increases. From cases 1 through 6, we observe that the number of subdivisions along both x and y influence $\hat{v}$, but only the increase of subdivisions along y yields a significant decrease in Z_0. Also shown in the table are the capacitance and inductance (represented by C and L), calculated from (6). We observe that the capacitance converges from below and the inductance converges from above as earlier speculated. The corresponding TEM structure (no y-directed conductors) has $C = 0.2578$ pf/mm and $L = 0.4331$ nh/mm. Although satisfactory for all the other cases, M given by (11) yields incorrect values for $\hat{v}$, Z_0, and the current distribution in case 4. Doubling M, however, gives the values listed in the table. From the table, the maximum changes in $\hat{v}$ and Z_0 are 0.14 and 3.6 percent, respectively. Cases 1 and 6 were repeated at high frequency ($k_\epsilon = 1.0$ mm^{-1}), and showed comparable rates of convergence.

Next, we truncated the infinite series in (3) and (5) at different points. We observed that doubling N in cases 1 and 5 produced changes in $\hat{v}$ and Z_0 of less than 0.01 and 0.04 percent, respectively. Doubling M in case 1 decreases $\hat{v}$ by 0.02 percent and decreases Z_0 by 0.72 percent, while doubling M in case 2 results in less than half the above changes—thus, once a fine enough subdivision along y is employed, using more modes than given by (11) yields only minimal improvements in accuracy.

To improve the convergence, a more non-uniform subdivision of the unit cell, one that employs narrow strips along the conductor edges to better represent current crowding, would undoubtedly give faster convergence (with respect to the number of subsections). An efficient algorithm for calculating the Z elements in (3), however, takes advantage of the occurrence of elements having repeated values. Though the total number of Z elements would be reduced, such a non-uniform subdivision might actually increase the number of elements having different values and, therefore, increase the computational expense.

VI. CONCLUSION

The propagation characteristics have been calculated for transmission line structures consisting of signal lines situated between a pair of mesh reference planes through the extension of a previous analysis involving a rooftop current approximation. The conductors have zero thickness, finite sheet resistance, and the dielectric is homogeneous.

A number of examples were considered for perfectly conducting structures at low frequency ($k_\epsilon d_1 \ll 1$). The results showed that the propagation velocity is just a few percent less than the speed of light in the dielectric, and that an array of crossing, orthogonal lines causes the propagation velocity and characteristic impedance to decrease (both by 3–4 percent for the structures considered). The crosstalk between adjacent signal lines was calculated, showing that the near-end coupled noise is greater for signal lines sitting side-by-side than for signal lines vertically adjacent but separated by a mesh plane (through-mesh case). The far-end noises were shown to be comparable, though the presence of crossing lines subsequently causes the side-by-side far-end noise to approximately double. The crosstalk, of course, is strongly dependent on the geometrical parameters defining the structure. The presence of y-directed conductors, whether as part of the mesh

planes or as crossing lines, significantly decreases the mutual capacitance between coupled lines, but has a negligible effect on the mutual inductances. A plot of the current distribution on a y-signal line showed the expected loop current flow necessary to cancel the magnetic field produced by the other conductors, giving additional support to the solution technique.

In calculating the L and C matrices, the telegraphist's equations, which hold true exactly for TEM transmission lines, were assumed to hold in the mesh-plane environment. This assumption was verified through a comparison of parameters calculated for mesh structures and for mesh structures devoid of y-directed conductors (so they become TEM structures). Excellent agreement (within 5 percent) was observed in the elements of the inductance matrix, the parameters least sensitive to the presence of y-directed conductors. The mutual capacitances in the mesh structure were substantially less, as expected. Though the changes in the self terms due to y-directed conductors in the mesh planes were small, they were in the direction opposite to that expected. This discrepancy, however, was attributed to the numerical error associated with the relatively coarse subdivision of the unit cell. The application of the telegraphist's equations were further supported through the close agreement between L_{12} and L_{21}, and between C_{12} and C_{21}; though calculated in the through-mesh structure as independent parameters, they exhibited the near reciprocal behavior expected in a near-TEM structure. Further support was provided through calculations of capacitance and inductance over a range in the height parameter h. These results indicated the same close agreements and trends for all the values of h considered.

The numerical convergence of the solution technique was examined by modifying the unit cell subdivision in a one-mesh-plane structure. Increasing, in different ways, the number of subsections by a factor of about four led to maximum changes of 0.14 percent in propagation velocity and 3.6 percent in characteristic impedance, with only an increase in the number of subsections along y significantly affecting the impedance. These results, along with our investigations of the two-mesh-plane structures, indicate that acceptable accuracy in $\hat{v}$ and coupled noise can be obtained with a relatively coarse subdivision. For structures that are very close to TEM, however, a finer subdivision along y may be required to distinguish clearly their values of Z_0, C_{11}, C_{22}, L_{11}, L_{22}, and L_{12} from those of their TEM counterparts.

The structures considered here have zero thickness. The approach, however, can be extended to handle thick conductors by using rooftop current elements to represent the current in the $x-z$ and $y-z$ planes.

Appendix

Expressions for $F_{x\alpha\beta}$ and $F_{y\alpha\beta}$

$$F_{x\alpha\beta} = \left\{ F_C \delta_{x_\alpha, x_\beta} + F_L \delta_{\tau_{v\alpha}+x_\alpha, x_\beta} + F_R \delta_{x_\alpha, \tau_{u\alpha}+x_\beta} \right\} \delta_{y_\alpha, y_\beta} \delta_{z_\alpha, z_\beta}$$

$$F_{y\alpha\beta} = \left\{ \frac{3}{8}(\tau_{f\alpha}+\tau_{g\alpha})\delta_{y_{P+\alpha}, y_{P+\beta}} + \frac{1}{8}\tau_{g\alpha}\delta_{\tau_{g\alpha}+y_{P+\alpha}, y_{P+\beta}} + \frac{1}{8}\tau_{f\alpha}\delta_{y_{P+\alpha}, \tau_{f\alpha}+y_{P+\beta}} \right\} \delta_{x_{P+\alpha}, x_{P+\beta}} \delta_{z_{P+\alpha}, z_{P+\beta}}$$

where

$$F_C = \frac{1}{j2k_x}\left[\exp(jk_x\tau_{u\alpha}/2) - \exp(-jk_x\tau_{v\alpha}/2)\right] + \frac{1}{\tau_{v\alpha}k_x^2}\left[1-\exp(-jk_x\tau_{v\alpha}/2)\right] + \frac{1}{\tau_{u\alpha}k_x^2}\left[1-\exp(jk_x\tau_{u\alpha}/2)\right]$$

$$F_L = \frac{1}{j2k_x}\exp(jk_x\tau_{v\alpha}/2) + \frac{1}{\tau_{v\alpha}k_x^2}\left[\exp(jk_x\tau_{v\alpha}/2)-1\right]$$

$$F_R = \frac{1}{-j2k_x}\exp(-jk_x\tau_{u\alpha}/2) + \frac{1}{\tau_{u\alpha}k_x^2}\left[\exp(-jk_x\tau_{u\alpha}/2)-1\right]$$

and $\delta_{u,v}$ is a modified form of the Kronecker delta, defined as

$$\delta_{u,v} = \begin{cases} 1, & u = v \\ 0, & \text{elsewhere.} \end{cases}$$

References

[1] A. J. Blodgett and D. R. Barbour, "Thermal conduction module: A high performance multilayer ceramic package," *IBM J. Res. Develop.*, vol. 26, 1, pp. 30–36, Jan. 1982.

[2] D. A. Hill, "Electromagnetic wave propagation along a pair of rectangular bonded wire meshes," *IEEE Trans. Electromagn. Compat.*, vol. EMC-21, pp. 114–122, May 1979.

[3] P. M. Grau, "The effect of crossing lines on electrical parameters of multi-conductor printed circuit hardware," Conference Rec., *Twelfth Asilomar Conf. Circuits Systems & Computers*, Nov. 1978, pp. 516–520.

[4] B. J. Rubin and H. L. Bertoni, "Waves guided by conductive strips above a periodically perforated ground plane," *IEEE Trans. Microwave Theory Tech.*, vol. MTT-31, pp. 541–549, July 1983.

[5] A. W. Glisson and D. R. Wilton, "Simple and efficient numerical methods for problems of electromagnetic radiation and scattering from surfaces," *IEEE Trans. Antennas Propagat.*, vol. AP-28, pp. 593–607, Sept. 1980.

[6] B. J. Rubin and H. L. Bertoni, "Reflection from a periodically perforated plane using a subsectional current approximation," *IEEE Trans. Antennas Propagat.*, vol. AP-31, pp. 829–836, Nov. 1983.

[7] K. D. Marx, "Propagation modes, equivalent circuits, and characteristic terminations for multiconductor transmission lines with inhomogeneous dielectrics," *IEEE Microwave Theory Tech.*, vol. MTT-21, pp. 450–457, July 1973.

[8] C. J. Anderson, "Electrical properties of an input-output cable for Josephson applications," *Rev. Sci. Instrum.*, vol. 53, pp. 1663–1666, Nov. 1982.
[9] A. Feller, H. R. Kaupp, and J. J. DiGracomo, "Crosstalk and reflections in high-speed digital systems," in *Proc. Fall Joint Computer Conf.*, Dec. 1965.
[10] W. T. Weeks, "Calculation of coefficients of capacitance of multiconductor transmission lines in the presence of a dielectric interface," *IEEE Trans. Microwave Theory Tech.*, vol. MTT-18, pp. 35–43, Jan. 1970.
[11] D. A. Reitan, "Accurate determination of the capacitance of rectangular parallel-plate capacitors," *Journ. Appl. Phys.*, vol. 30, pp. 172–176, Feb. 1959.

Barry J. Rubin (S'72–M'74–M'82) was born in New York, NY, in 1952. He received the B.E.E.E. degree from the City College of New York, New York, in 1974.

He joined the International Business Machines Corporation in 1974 and received the M.S.E.E. degree from Syracuse University, Syracuse, New York, in 1978 and received the Ph.D. degree from the Polytechnic Institute of New York, Brooklyn, in 1982. He has worked on power transistor design, CCD technology, circuit design and, since 1976, on electrical packaging analysis. He has been awarded five US patents.

Computer Analysis of Dielectric Waveguides: A Finite-Difference Method

EDGARD SCHWEIG, MEMBER, IEEE, AND WILLIAM B. BRIDGES, FELLOW, IEEE

Abstract—**A method for computing the modes of dielectric guiding structures based on finite differences is described. The numerical computation program is efficient and can be applied to a wide range of problems. We report here solutions for circular and rectangular dielectric waveguides and compare our solutions with those obtained by other methods. Limitations in the commonly used approximate formulas developed by Marcatili are discussed.**

I. Introduction

DIELECTRIC WAVEGUIDES of high permittivity ($\epsilon_r' \gtrsim 10$) have been proposed as practical waveguiding structures for use in millimeter-wave integrated circuits (MMIC) [1], [2]. The prospect that the dielectric material could be a high-resistivity semiconductor raises the further possibility that active devices could be fabricated directly into the transmission line. Various practical devices for millimeter-wave applications utilizing dielectric waveguides also have been suggested: directional couplers [3], balanced mixers [3], phase shifters [4], [5], scanning antennas [6], channel-dropping filters [7]. The theoretical analysis of these devices has been based, in the case of rectangular guides, on the analytical solutions proposed by Marcatili [8], which can be expressed in simple closed forms. However, Marcatili's quasi-plane-wave analysis is based on assumptions that are not met when the permittivity of the guide is high compared to the outer medium.

Several authors have proposed methods for the study of rectangular guides: Knox *et al.* [1] (modification of Marcatili's analysis), Goell [9] (expansion in circular harmonics), Schlosser [10] and Solbach [11] (mode matching), and Yeh [12], [13] (finite elements). With the exception of Solbach [11], they limit their analyses to relatively small values of permittivity ($\epsilon_r' \simeq 2.5$) and they do not give the field distributions calculated by their methods.

We have developed a numerical technique based on finite differences (FD) for computing accurate dispersion characteristics and field distribution for dielectric waveguides. This method is computationally more efficient than finite elements (FE), thus allowing the use of finer meshes, a desirable feature when accurate values of the fields are required.

II. Variational Formulation

Both the finite-elements method (FE) and the finite-difference method (FD) are based on a variational principle [14], [19]. For one-dimensional problems, the two methods are equivalent [15]. This equivalence is maintained in two-dimensional problems that have simple rectangular boundaries. The advantages of a variational approach are: 1) the method does not restrict the shape of the dielectric interfaces so that complicated dielectric cross-sectional profiles can be treated; 2) the procedure is numerically stable; and 3) it permits the use of a graded mesh that can

Manuscript received July 7, 1983; revised December 15, 1983. This work was supported by the Office of Naval Research under Contract N00014-79-C-0-0839.

The authors are with the California Institute of Technology, Department of Electrical Engineering, Pasadena, CA 91125.

0018-9480/84/0500-0531$01.00 ©1984 IEEE